A fast and general method to empirically estimate the complexity of distributed causal interactions in the brain

Renzo Comolatti[1], Andrea Pigorini[2], Silvia Casarotto[2], Matteo Fecchio[2], Guilherme Faria[1], Simone Sarasso[2], Mario Rosanova[2], Olivia Gosseries[3,4], Mélanie Boly[5], Olivier Bodart[3,4], Didier Ledoux[3], Jean-François Brichant[6], Lino Nobili[7], Steven Laureys[3,4], Giulio Tononi[5], Marcello Massimini[2,8¶], Adenauer G. Casali[1¶*]

[1]Institute of Science and Technology, Federal University of São Paulo, São José dos Campos, Brazil

[2]Department of Biomedical and Clinical Sciences "Luigi Sacco", University of Milan, Milan, Italy

[3]GIGA-Consciousness, GIGA Research, University of Liège, Liège, Belgium

[4]Coma Science Group, University Hospital of Liège, Liège, Belgium

[5]Department of Psychiatry, University of Wisconsin, Madison, USA

[6]Department of Anesthesia and Intensive Care Medicine, University Hospital of Liège, Liège, Belgium

[7]Center of Epilepsy Surgery "C. Munari", Department of Neuroscience, Niguarda Hospital, Milan, Italy

[8]Istituto Di Ricovero e Cura a Carattere Scientifico, Fondazione Don Carlo Gnocchi, Milan, Italy.

*Corresponding author. E-mail: casali@unifesp.br

¶These authors contributed equally to this work

Abstract

A novel metric, called Perturbational Complexity Index (PCI), was recently introduced to assess the capacity of thalamocortical circuits to engage in complex patterns of causal interactions. Once validated and calibrated in a large benchmark, PCI showed high accuracy in detecting consciousness in brain injured patients. In its original formulation, the index was computed by stimulating the brain with transcranial magnetic stimulation (TMS) and using the Lempel-Ziv algorithm to quantify the spatiotemporal complexity of cortical responses, as derived by the inverse solution of high-density EEG (hd-EEG). Despite its accuracy in assessing consciousness, the original formulation of PCI was limited by its reliance on source estimation, which not only renders its calculation time-consuming, dependent on elaborate experimental setups and offline processing, but also restricts its extension to other types of brain signals beyond TMS/hd-EEG recordings. Here, we address these limitations and introduce PCI^{ST}, a fast and simple method for estimating perturbational complexity of any given brain response signal. Our approach combines dimensionality reduction with a novel metric of complexity derived from recurrence quantification analysis, in which state transitions (ST) present in the signal's principal components are quantified in order to estimate spatiotemporal complexity directly at the sensors level. PCI^{ST} was tested on a large dataset of TMS/hd-EEG recordings obtained from 108 healthy subjects and 108 patients with brain injuries, and also applied to sparse intracranial recordings of 9 patients undergoing intra-cerebral single-pulse electrical stimulation. The new method performs with the same accuracy as the original formulation, but the index can be computed in less than a second, requires a simpler setup and can be generalized to sparse intracranial recordings. PCI^{ST} advances towards the development of a clinical bedside index of consciousness and can be used as a general tool to study the brain's complexity across scales, experimental models and species.

Introduction

Measures of brain complexity have recently begun to move from the realm of theoretical neuroscience [1-6] into the field of experimental neurophysiology to study differences between global brain states, from wakefulness to sleep and anesthesia [7-10]. Further, measures of brain complexity have been considered as useful paraclinical indices to assess consciousness at the bedside of brain-injured patients [11-15]. In this spirit, a novel strategy based on quantifying the global effects of direct cortical perturbations was recently introduced [16]. This approach is motivated by the general theoretical principle that a brain's capacity for conscious experience relies on its ability to integrate information [5]. In this view, a key mechanism of consciousness is the ability of different neural elements to engage in complex patterns of causal interactions such that the whole system generates information over and above its parts.

Practically, in order to estimate the amount of causal, irreducible information that a system can generate, a general procedure was implemented based on two steps: (i) locally perturbing the system in a controlled and reproducible way to trigger a cause-effect chain and (ii) quantifying the spatiotemporal complexity of the ensuing deterministic response to estimate information. The original implementation of this perturb-and-measure approach [16] involved (i) stimulating the brain with transcranial magnetic stimulation (TMS) and (ii) computing the algorithmic (Lempel-Ziv) complexity of the resulting patterns of activations at the level of cortical sources derived from the inverse solution of high-density electroencephalographic (hd-EEG) responses; this metric will be henceforth referred to as Lempel-Ziv Perturbational Complexity Index (PCI^{LZ}).

Albeit macroscopic and coarse, PCI^{LZ} provided maximum (100%) accuracy in detecting consciousness in a large (n=150) benchmark population of subjects who could confirm the

presence or absence of conscious experience through immediate or delayed reports. PCI^{LZ} was lower in all unresponsive subjects who did not report any conscious experience upon awakening from non-rapid eye movement (NREM) sleep or midazolam, xenon, and propofol anesthesia, and was invariably higher in conditions in which consciousness was present, including awake controls, conscious brain-damaged patients and subjects who were disconnected and unresponsive during dreaming and ketamine anesthesia but retrospectively reported having had vivid conscious experiences upon awakening [17, 18]. Once calibrated on the gold-standard of subjective reports, PCI^{LZ} measurements performed at the bedside of non-communicating subjects with brain injuries offered high sensitivity (94%) in detecting minimally conscious patients and allowed identifying a significant percentage (about 20%) of vegetative state/unresponsive wakefulness syndrome (UWS) cases with high brain complexity, who had a higher chance of eventually recovering consciousness [17].

While PCI^{LZ} performs with unprecedented accuracy, it also has practical drawbacks and limitations. First, PCI^{LZ} can only be computed on spatiotemporal matrices of cortical activations that are obtained after an intensive processing of TMS/hd-EEG data, including forward modeling [19], source estimation [20] and permutation-based statistics at the single-trial level. All these steps imply a complicated and lengthy off-line analysis pipeline that hinders the dissemination of the method and its application as a routine clinical bedside tool. Clearly, the possibility of estimating perturbational complexity directly at the level of EEG sensors, may have critical advantages: not only it would render the analysis process faster (ideally, on-line), easier to standardize and immune to the technical caveats of source modeling, but it would also allow the use of simplified and cheaper set-ups (i.e. not requiring hd-EEG and subject-specific MRI scans).

A second important drawback of PCI^{LZ} is its limited application to signals other than TMS/hd-EEG evoked potentials. Intracranial stimulations/recordings in humans [21, 22] and in animal models[23-26] as well as intra and extracellular responses recorded from cortical slices [27, 28] offer an unprecedented range of opportunities to elucidate the relationships between neuronal dynamics, network complexity and consciousness [29]. However, because PCI^{LZ} relies on EEG source estimation, its extension to other types of recordings, such as sparse matrices of intra-cerebral stereo EEG recordings and in vivo/in vitro local field potentials, is not straightforward [27].

Here we propose a novel measure of perturbational complexity that bears conceptual similarities with PCI^{LZ} but is much faster to compute and in principle generalizable to any type of brain signal evoked by perturbations or event related. Conceptually, we started from the notion that the binary sequences of activation and deactivations which are compressed by PCI^{LZ} can be considered as sequences of transitions between different states: a "response state" and a "non-response" or "baseline state". Thus, one should expect to find high values of perturbational complexity in systems that react to the initial perturbation by exhibiting multiple and irreducible patterns of transitions between response and non-response states. Following this intuition, we here introduce PCI^{ST}, an index that combines dimensionality reduction and a novel metric of recurrence quantification analysis (RQA) to empirically quantify perturbational complexity as the overall number of non-redundant state transitions (ST) caused by the perturbation.

We validated PCI^{ST} on a large dataset of 719 TMS/hd-EEG sessions recorded from 108 healthy subjects during wakefulness, NREM sleep and anesthesia (propofol, midazolam and xenon) as well as 108 brain-injured patients with disorders of consciousness (DOC). Furthermore, we applied the same index to 84 stereotactic EEG recordings (SEEG) obtained in 9

epileptic patients undergoing intra-cerebral single-pulse electrical stimulation (SPES) during both wakefulness and sleep for clinical evaluation. The index was able to approximate the performance of PCI^{LZ} in healthy subjects and patients, while improving on the previous method by dispensing with both source estimation and permutation statistics, being computed in less than a second; further, its application generalizes from the scalp EEG to sparse intracranial recordings thus potentially enabling the exploration of the complexity of the brain's causal structure across scales, experimental models and species.

Results

Overview of the method

In the original formulation [16], perturbational complexity was calculated by binarizing TMS-evoked potentials (TEPs) at the EEG sources level using a fixed threshold derived from non-parametric statistics with respect to the baseline (pre-stimulus) and subsequently compressing the binary spatiotemporal patterns with the Lempel-Ziv algorithm. An underlying assumption of this binarization strategy is that complex activations engaged by the perturbation appear on the evoked signals as patterns of oscillations around a fixed amplitude scale. Although proven successful when applied to the sources level, this approach is less sensitive in detecting complexity when calculated directly at the EEG-scalp level, where fast oscillations can appear riding on top of larger and slower envelopes as result of volume conduction and signal mixing (S1 Fig). Furthermore, complex neuronal oscillations occurring in amplitude scales that are not determined by a fixed threshold can also be observed in microscopic and mesoscopic recordings due to cross-frequency couplings [30-34], and a binarized measure applied to such scales would have limited applicability to detect complex physiological activations.

Aiming at a general index of perturbational complexity that can be fast and efficiently calculated directly at the EEG-sensors level, we here took a non-binary, geometrical approach and tried to quantify the spatiotemporal complexity of evoked potentials by exploring multiple amplitude fluctuations present in the response. At the scalp level, TEPs appear as time-varying voltage configurations, with local maxima shifting over time across different EEG sensors [16]. When voltages of all electrodes are put together in a vector space, TEPs can be geometrically represented by a trajectory in the so called EEG space [35]. Fig 1 depicts examples of these trajectories for 60-channels TEPs recorded during alert wakefulness and NREM sleep, after projecting the data in a lower dimensional space spanned by the first three principal components (PCs) of the evoked response. Contrary to the trajectories observed during NREM sleep, which are either local and short-lasting (Fig 1B) or widespread and non-recurrent (Fig 1C), complex TEPs recorded during wakefulness appeared in the principal components' space as entangled, interlaced paths (Fig 1A). In this geometrical approach, estimating perturbational complexity becomes a matter of quantifying the complexity of these trajectories.

The state transition based perturbational complexity index (PCI^{ST}) estimates complexity by quantifying transitions between states within the trajectory spanned by the system's response to a perturbation. In the following, we summarize the steps involved in calculating PCI^{ST} (see Materials and Methods for further details). Starting from trial-averaged signals recorded in response to a perturbation, principal component analysis (PCA) of the response is performed in order to effectively reduce the dimension of the data (Fig 2A). The complexity of each resulting principal component is then evaluated by quantifying what we call *state transitions*, using a method derived from RQA[36, 37]. In order to do so, distance matrices, defined by the voltage-amplitude distances between all time-points of the signal, are calculated separately for pre-

stimulus and post-stimulus samples (Fig 2B). These 2D distance matrices provide a summary of the geometrical relationships of the baseline and the response signals. By thresholding both distances matrices (baseline and response, Fig 2C) at a given scale ε, we obtain a contour plot, called the transition matrix, that depicts the temporal transitions between states – roughly, the ups and downs in the signal –, for both the baseline and the response (Fig 2D). By varying the threshold ε and comparing the number of state transitions (NST) in the matrices of the response with that of the baseline, we can look for the scales at which there are state transitions in the signal's response over and above transitions present in the baseline activity (Fig 2E). The complexity of each component (red dot in Fig 2E) thus becomes the weighted difference of NST (ΔNST) between baseline and response signals calculated at the threshold ε* where this value is maximum. Finally, PCI^{ST} is defined as the sum of these maximized significant state transitions across all principal components of the evoked signal.

By its definition, PCI^{ST} is high when there are multiple linearly independent components in a spatially distributed response (spatial complexity), each one of them contributing with significant amounts of state transitions (temporal complexity). Conversely, PCI^{ST} is expected to be low either if the perturbation evokes a strongly correlated response across different spatial recordings or if the independent components carry few temporal transitions in the response as compared to the baseline.

PCI^{ST} is reliable and fast in benchmark conditions

PCI^{ST} was calculated on a benchmark of 382 TEPs obtained in a group of 108 subjects during conscious (alert wakefulness) and unconscious (NREM sleep and anesthesia) conditions (Fig 3A). The wakefulness group presented significantly higher and more variable PCI^{ST} values

(mean ± SD, 47.89 ± 12.65) than the NREM sleep/anesthesia group (mean ± SD, 14.19 ± 5.26, $p = 4.7x10^{-40}$, Wilcoxon-ranksum test). In terms of classification performance between conscious and unconscious conditions, PCI^{ST} showed a high classification power that was equivalent to the performance of the original version of PCI in this same dataset [17] (area under the curve (AUC) of the receiver-operator characteristics (ROC) for PCI^{ST} =0.998, AUC for PCI^{LZ} = 0.995). Indeed, when values for each TMS/hd-EEG session were compared, we found a significant linear correlation between the metrics (r = 0.82, $p<10^{-95}$, Fig 3B). On the other hand, because PCI^{ST} estimates perturbational complexity without employing source localization and surrogate techniques, a key difference found was that PCI^{ST} computation on the whole benchmark dataset was approximately 380 times faster than with PCI^{LZ}. While PCI^{LZ} took about 300 seconds per session to compute (mean ± std, 270s ± 99), PCI^{ST} was calculated in less than one second (mean ± std, 0.71 ± 0.20, $p< 10^{-127}$) (Fig 3C).

PCI^{ST} captures spatiotemporal complexity as the joint presence of spatial independence and temporal complexity

PCI^{ST} is the product between the number of selected principal components (N_C) of the evoked response and the average number of state transitions across all its components ($\overline{\Delta NST}$). The first quantity can be regarded as a measure of the underlying dimensionality of the data and is calculated as the number of linearly independent components that span most of the evoked response in terms of its square amplitude and signal-to-noise ratio. In the case of the TMS/hd-EEG signals, N_C is high when different EEG sensors record different evoked potentials and, therefore, it can be viewed as a measure of the *spatial differentiation* of the brain's response to the perturbation. The second quantity, $\overline{\Delta NST}$, corresponds to the average *temporal complexity*

present in the individual principal components as measured by the quantification of state transitions. Thus, $\Delta\overline{NST}$ is high when the signal's response displays a variety of patterns of activations across time over and above the patterns occurring before the stimulation onset.

At the group level, TEPs recorded during alert wakefulness presented both significantly higher number of principal components N_C (mean ± SD, 7.16 ± 1.41 vs 4.04 ± 0.94, p = 4.20 x 10^{-36}) and $\Delta\overline{NST}$ values (mean ± SD, 6.69 ± 1.21 vs 3.47 ± 0.89, p = 4.20 x 10^{-38}) than the TEPs in unconscious conditions (Fig 4A). Taken separately, the metrics displayed a higher overlap between the conscious and unconscious distributions (N_C: AUC=0.966, FDR = 3.40; $\Delta\overline{NST}$: AUC=0.985, FDR = 4.60) than when combining them through their product (PCI^{ST}: AUC=0.998, FDR = 6.07 , Fig 3A).

Each *n*th principal component contributes to PCI^{ST} with its correspondent ΔNST_n value. Fig 4B shows the ΔNST_n distributions for conscious and unconscious conditions, ordered by eigenvalues of the selected components. Importantly, ΔNST_n showed no positive bias toward lower eigenvalue components as could be expected by the higher frequency content of these components. In fact, ΔNST_n in consciousness remained relatively stable across all components. Notably, for each single component, ΔNST_n values in signals from conscious individuals were, on average, significantly higher than the correspondent values in the unconscious condition: wilcoxon-ranksum comparisons between conscious and unconscious conditions across the first 5 components resulted in p-values always lower than 10^{-9}.

PCI^{ST} dependence on sampling frequency, number of EEG channels and number of TMS trials

We next tested the influence of TMS/hd-EEG recording parameters on PCI^{ST} values.

Sampling Frequency. To determine the dependence of PCI^{ST} on the sampling frequency, TEPs were resampled from the original 725Hz down to 200Hz, which is above the Nyquist rate of the signals, and the index was calculated accordingly. Classification power and distance between conscious and unconscious distributions were stable across different sampling frequencies (AUC =0.998 and FDR ranging between 6.02 and 6.32, Fig 5A, top). Notably, there were no significant effects of sampling frequency on average values of PCI^{ST}, which remained stable in both conscious and unconscious conditions (Fig 5A, bottom).

Number of EEG trials. Next, we evaluated the dependence of PCI^{ST} on the number of trials employed to construct the TEPs. PCI^{ST} was tested on surrogate TEPs generated with different numbers of selected trials (n_t) from the original data. As the TMS/hd-EEG sessions had varying numbers of trials, only those sessions that have at least 200 TMS stimulation trials were selected from the benchmark dataset totalizing 117 sessions from 67 subjects. Then, for a given n_t considered, 25 surrogates of each session's TEP were generated by averaging n_t randomly selected trials; PCI^{ST} was then calculated on all surrogates and the average value across all surrogates was used as the metric for the given session.

Repeated measures ANOVA showed significant effects of the number of trials ($F_{6,107}$ = 60.42, $p = 3.9 \times 10^{-35}$) and a significant interaction with the level of consciousness ($F_{6,107} = 21.31$, $p=2.5 \times 10^{-16}$). The addition of trials amplified stimulus-locked potentials that are present during wakefulness but absent in NREM sleep and anesthesia: PCI^{ST} remained almost constant regardless of the number of trials used for the evoked potentials in unconscious conditions but

increased sharply with the number of trials in wakefulness (Fig 5B). The estimation of the marginal means indicated a significant growth across successive steps of 25 trials in wakefulness up to 150 trials (95% confidence interval).

From the classification perspective, although the FDR of the PCI^{ST} distributions for the benchmark dataset increased steadily with the number of trials, the classification power measured by AUC saturated early at 125 trials (AUC=0.999, FDR = 7.26) (Fig 5B).

Number of EEG channels. From a practical perspective, the minimum number of scalp electrodes required to adequately estimate the spatiotemporal complexity of brain EEG responses is a most relevant factor. The use of hd-EEG, besides entailing more expensive hardware, involves a cumbersome and lengthy preparation, resulting in limited applicability, especially in the clinical set-up. While PCI^{LZ} necessarily demands hd-EEG systems so as to accurately perform source localization, PCI^{ST} can in principle be calculated on a reduced number of channels. We thus compared the performance of the index calculated on the original hd-EEG system (60 channels) to reduced setups containing 19 and 8 electrodes.

Notably, PCI^{ST} revealed an equivalent performance to discriminate conscious from unconscious conditions in the benchmark when calculated on 19-channels distributed accordingly to a standard 10-20 EEG system as compared to the high-density setup (linear correlation $r = 0.962$, $p = 6.4 \times 10^{-216}$; AUC=0.997, FDR=6.11, Fig 5C-top). Still, repeated measures ANOVA indicated that the reduced 19 channels dataset yielded consistently lower values of PCI^{ST} ($F_{1,379} = 94.00$, $p = 5 \times 10^{-20}$). This reduction was more pronounced for the wakefulness group, as shown by the significant interaction with the state of consciousness ($F_{1,379} = 47.32$, $p = 2.4 \times 10^{-11}$), suggesting that, in spite of an accurate discrimination, the reduced 10-20 set-up may fail to capture part of the structure of complex responses.

These effects were more prominent when PCI^{ST} was calculated on a subset of the 10-20 EEG system containing only 8 channels (Fig 5C-bottom). In this case, the simpler setup resulted in average loss of complexity for the wakefulness group of 27.8% with respect to the values obtained using the original hd-EEG system (repeated measures: $F_{1,379} = 280.63$, $p = 1x10^{-47}$; interaction with the condition of consciousness $F_{1,379} = 144.83$ $p = 2x10^{-28}$) and, yet with just a slightly lower classification accuracy (AUC = 0.992, FDR = 5.92).

PCI^{ST} allows a simple and fast set-up at the bedside of patients

After ascertaining the effectiveness of PCI^{ST} to discriminate consciousness from unconsciousness in healthy subjects while dispensing both source estimation and hd-EEG, we tested the performance of the novel index in 108 brain-injured patients with disorders of consciousness (DOC). For each EEG setup (60, 19 and 8 channels, Figure 5C), thresholds discriminating consciousness from unconsciousness were extracted from the PCI^{ST} values of the benchmark population using a linear classifier [38] (see Materials and Methods and S2 Fig). These empirical cutoffs were then compared to PCI^{ST} values obtained from a group of brain-injured patients who had recovered from coma and evolved toward various clinical conditions: Unresponsive Wakefulness Syndrome (UWS, N=43), Minimally Conscious State (MCS, N=49), patients who had emerged from Minimally Conscious State (EMCS, N=11) and conscious subjects affected by the Locked-In Syndrome (LIS, N=5). As the patient's capacity for consciousness is the crucial question of clinical relevance in this population, we followed the previous approach [17] and classified each patient using his maximum PCI^{ST} value (PCI^{ST}_{Max}) obtained across all recorded sessions.

When calculated on the original high-density setup, the sensitivity of PCI^{ST} in detecting signs of consciousness in brain-injured patients was comparable to PCI^{LZ} [17] (Fig 6A, top): PCI^{ST} made no erroneous classifications on conscious (LIS/EMCS) brain-injured patients and achieved 91.9% sensitivity among minimally conscious individuals, correctly detecting signs of consciousness in 45 from 49 MCS patients (see S3 Fig for individual values of PCI^{ST}). Notably the performance of the index diminished only slightly with the use of the standard 10-20 EEG system (19 channels), yielding sensitivities of 100% and 89.8% (44/49) for EMCS/LIS and MCS respectively (Fig 6A, middle). Finally, the simpler 8-channels setup resulted in reduced sensitivity scores on both EMCS/LIS (94%) and MCS (84%) patients (Fig 6A, bottom).

In UWS patients, the absence of behavioral signs of consciousness per se cannot be considered a proof of the absence of consciousness. Thus, brain-based measures that do not require subject's interaction with the external environment can be useful to detect a covert capacity for consciousness. In a previous study, PCI^{LZ} detected conscious-like complexity in 20.9% (9/43) of UWS patients, who also had a higher chance of recovery at 6 months [17]. Here, we evaluated whether these patients could also be identified by PCI^{ST}. The novel index calculated on both high-density and standard 10-20 EEG setups detected all (n=9) the patients with high PCI^{LZ}, whereas more than 82% of patients classified as low-complexity by PCI^{LZ} were also below threshold for PCI^{ST} (hd-EEG: 88.2%, 10-20 setup: 82.3%, Fig 6B-top and middle). The simpler 8-channels setup detected 8 out of 9 (88.9%) high-complexity patients and 29 out of 34 (85.3%) low-complexity patients (Fig 6B, bottom).

PCI^{ST} can be generalized to intracranial responses

Given that PCI^{ST} estimates perturbational complexity directly at the level of sensors, its extension to other types of recordings is straightforward. As a proof of concept, we calculated PCI^{ST} on sparse intracranial SEEG recordings in 9 patients undergoing presurgical mapping for epilepsy. In each patient, SEEG responses evoked by single-pulse electrical stimulation (SPES) of different contacts were recorded both during wakefulness and NREM sleep, resulting in a total of 84 sessions (see S1 Table).

Fig 7 illustrates the results obtained for two stimulation sessions in a representative subject and shows how PCI^{ST} can quantify changes of spatiotemporal complexity in SPES/SEEG responses across brain states. Specifically, during wakefulness, the composite set of waves elicited by SPES appeared as a large number of components characterized by recurrent waves of activity in the principal components space, which resulted in high PCI^{ST} values. On the other hand, during NREM sleep, when SPES evoked a stereotypical wave, a small number of components were enough to span most of the response. In addition, the few components that survived dimensionality reduction in NREM sleep showed less state transitions than the ones in wakefulness and accounted for a reduced PCI^{ST} value.

These findings were reproducible across stimulation sites and consistent at population level (Fig 8). PCI^{ST} during NREM sleep was lower than in wakefulness for each one of the 42 different stimulation sites (Fig 8A-I). Overall, compared to wakefulness, PCI^{ST} was reduced during NREM sleep on average by 46.5% (Fig 8J) and significant at the group level ($p = 4.7 \times 10^{-7}$, Wilcoxon-ranksum).

Discussion

In this paper we have developed and tested a new method of estimating pertubational complexity based on dimensionality reduction and state-transitions quantification. The novel index, called PCI^{ST}, represents a fundamental advancement towards the implementation of a reliable and fast clinical tool as well as a general measure than can be employed to explore the neuronal mechanisms of loss/recovery of brain complexity across scales and models.

PCI combines a "perturb and measure" approach with a complexity metric in order to empirically estimate the amount of irreducible information generated through causal interactions within a system [16, 39]. This approach is unique because it permits, at least in principle, to explore the structure of causal interactions from the intrinsic perspective of the system under study, above and beyond the patterns of correlations that can be appreciated by a purely extrinsic, observational perspective [5, 40]. Further, by measuring the average response evoked by repeated stimulations of the same cortical target, only the effects causally related to the perturbation are amplified, whereas unrelated patterns of activity are averaged out. In this way, it is possible to explore effective interactions while minimizing the effect of noise, common drivers and elements that are causally segregated. Finally, to estimate the complexity of intrinsic causal interactions, only the irreducible (i.e. non-redundant) patterns of spatiotemporal significant activity are considered. Perturbational complexity is both spatial and temporal in nature inasmuch as it is only produced when different elements interact causally in an integrated and differentiated manner. In practice, perturbational complexity is high only when a perturbation propagates reliably over a set of integrated elements that react differently, giving rise to a transient response encompassing a variety of irreducible spatiotemporal patterns of activation.

In the case of PCI^{ST}, this transient response is interpreted as a trajectory in the multidimensional space spanned by the sensors. For example, the TMS-evoked trajectory rests in the sensor space defined by the EEG channels (Fig 1). Mutanen et al. [35] has recently studied the ability of TMS to modulate brain activity by considering single-trial EEG responses to TMS as trajectories in the EEG signal space. Here we extended this geometrical approach and looked at the trajectories spanned by the evoked (trial-averaged) potentials in the rotated basis defined by the principal components of the response (Fig 1). PCI^{ST} quantifies perturbational complexity by estimating the spatiotemporal complexity of these evoked trajectories.

As a first step in this procedure, singular value decomposition (SVD) is used to rotate the trajectories into an orthonormal basis and optimally project them onto a space of lower dimension. This approach is similar to the concept of spatial PCA [41, 42], a data-driven technique that has been widely applied to evoked potentials [43-49] and that can be used to estimate the dimensionality of the trajectories in the EEG space in terms of the number of principal components accounting for the variance of the evoked response [50]. However, dimensionality reduction as operationalized in PCI^{ST} differs from spatial PCA in two important ways: (i) PCI^{ST} calculates SVD exclusively from the post-stimulus signals; (ii) the projection is based not on the covariance but on the correlation across sensors. This procedure guarantees that the principal components, onto which the evoked trajectories are projected, optimally explain the data in terms of the strength (mean field power) of the responses to the perturbation. As expected, when projected onto the space spanned by the components that accounts for most of the response strength, TEPs recorded from healthy awake subjects, which invariably present high value of perturbational complexity as assessed by PCI^{LZ}, were found to have significantly

higher-dimensional trajectories as compared to responses obtained in unconscious conditions (Fig 3).

While the number of selected principal components captures the spatial linear independence present in the response, the estimation of spatiotemporal complexity must also take into account the temporal information content present in each component. Since the complexity metric employed in the Lempel-Ziv formulation of perturbational complexity was based on binarizing temporal patterns with respect to a fixed significance threshold, PCI^{LZ} shows a reduced performance when calculated in the absence of source modeling, such as in scalp EEG, when fluctuations of different frequencies relying on distinct neural mechanisms may appear linked due to volume conduction. In this case, complex patterns riding on top of larger and slower components may be easily missed (see S1 Fig). Crucially, sensitivity to cross-frequency patterns of fast oscillations that are modulated by slower envelopes are particularly important because they have been reported at multiple levels, from microscopic to macroscopic recordings [30-34, 51], and because they may serve as the mechanism to coordinate neural dynamics and transfer information across spatial and temporal scales [52-55].

One way to explore the multiple amplitude scales of the activations in a time-series is by calculating its distance matrix [36, 56], which provides a summary of the geometrical relationships of the signal, not only in respect to the baseline but to every time point of the signal. Here, we proposed to quantify temporal complexity by binarizing not the original time-series but its corresponding distance matrix: a technique known as recurrence quantification analysis [36, 37]. Recurrences are typically present in complex dynamical systems [57]: eventually every system will return to a state which is sufficiently close to a previous one and quantifying these recurrent states have been shown to be an effective way to detect rhythms and

state changes within complex, possibly non-stationary, time-series [58-63]. Although inferring recurrences in the "true" state space of a dynamical system from a given time-series depends on properly choosing the embedding parameters to reconstruct the system's dynamical attractors [64] (see Materials and Methods), recurrence techniques are employed in calculating PCI^{ST} simply to quantify patterns in the time-series, without assuming that the underlying attractors are faithfully reconstructed. Indeed, it has been shown that, when applied to experimental data, recurrence plots and the measures derived from them are able to quantify patterns in the dynamics even if no embedding is performed [65]. In the case of PCI^{ST}, independence on embedding dimension has been substantiated by the fact that the performance of the method in discriminating between brain states was found to be stable across different embedding parameters (see S4 Fig).

In the context of RQA, several metrics were proposed to quantify the complexity of the dynamics [36], such as the diagonal-line based entropy [63], the recurrence probability density entropy [66] or the Kolmogorov-Sinai entropy [67]. Although detecting recurrent states does not require signals to be stationary, these metrics are based on statistical properties of densities of recurrent states and may be unreliable in estimating complexity of very short and highly non-stationary time series, such as those evoked by a perturbation. We here took a different perspective by simply counting the number of transitions between recurrent and non-recurrent states (NST) in the principal components space as a measure of the information content of the response to a perturbation. Notably, as this approach might be sensitive to patterns with a regular temporal structure that do not contribute to complexity as measured by compression-based metrics, PCI^{ST} can be expected to accurately estimate complexity only when applied to transient short-lasting signals, such as evoked potentials, in which regular patterns repeating over a long

time are unlikely to occur. Future studies in simulated dynamical systems [68, 69] and brain network models [2, 70, 71] should investigate to which extent counting state transitions with PCI^{ST} is enough to capture the complexity of the causal structure of a system.

Empirically, PCI^{ST} performed well in the case of the brain, which generates large-scale complex activations in response to a local perturbation in the form of short and transient oscillations with highly non-stationary frequencies. Indeed, PCI^{ST} was strongly correlated to PCI^{LZ} and reliably discriminated consciousness from unconsciousness in the large benchmark population of healthy individuals (Fig 3). Furthermore, and similarly to PCI^{LZ}, the absolute values of PCI^{ST} could be used to compare healthy subjects to brain-injured patients who emerged from coma. When applying the threshold derived from the benchmark population to individual brain-injured patients, PCI^{ST} exhibited high sensitivity in detecting consciousness (Fig 6), with a performance comparable to PCI^{LZ}.

This performance was achieved by dispensing with source estimation, forward modeling and non-parametric statistics, thus entailing several practical advantages. First and foremost, PCI^{ST} calculation takes less than one second per session (Fig 3), thus being more than three hundred times faster than PCI^{LZ}. Further, PCI^{ST} can afford an accurate estimation of perturbational complexity even on a reduced (standard 10-20) EEG set-up in both the healthy and brain-injured populations (Figs 5 and 6). Taken together, these advances pave the way to the implementation of a practical, fast and potentially online method to be applied at the bedside in the routine clinical setting.

Beside these practical applications, estimating perturbational complexity based on state transitions enables the exploration of the brain's causal structure across different recordings scales, from macroscopic EEG signals, to mesoscopic local field potentials and, in principle, to

microscopic multisite electrophysiological/optical recordings. In the present study we investigated this possibility at the mesoscale level by computing PCI^{ST} on intracranial SPES-evoked potentials. This novel metrics was able to detect systematic relative differences in brain complexity between wakefulness and sleep despite the substantial differences between the intracranial (SPES/SEEG) and non-invasive (TMS/EEG) recordings. First, the type of perturbation essentially differs from TMS in that bipolar intracranial SPES not only activates superficial fibers but also deep white matter as well as cell bodies [72] and it does so at a scale of millimeters. Second, the spatial distribution of the recording SEEG electrodes is sparse rather than arranged along a regular spatial matrix. Third, the local field potentials recorded by SEEG electrodes reflect the activity of neuronal assemblies than are substantially smaller than the ones sampled by scalp electrodes [73, 74]. Finally, SEEG can reach deep structures, such as hippocampus, amygdala and cingulate cortex [75] that cannot be directly accessed with TMS/EEG experiments.

In addition to the differences listed above, SPES presents key advantage over TMS in that the first is not associated with concurrent auditory and/or somatosensory stimulation [76]. Indeed, when not appropriately controlled for, these additional peripheral inputs induced by TMS may add to the EEG response, thus confounding the genuine effects of direct cortical stimulation [77, 78]. In this respect, the present intracranial results serve as a definite confirmation of the fundamental interpretation of perturbational complexity, as originally assessed through TMS/hd-EEG recordings. As shown in Fig 7, direct intracortical stimulation elicited significant transitions contributing to the build-up of PCI^{ST} that occurred both at short and long latencies, beyond 300 milliseconds and that were specific for the stimulation site. Thus, the differences in PCI^{ST}

between wakefulness and sleep reflect genuine changes in the intrinsic causal properties of thalamocortical circuits, unconfounded by the effects of state-dependent sensory input gating.

Most important, PCI^{ST} allows the exploration of the mechanisms of brain complexity at the finer scale of circuits and neuronal mechanisms. For example, at the level of the intracranial stimulation/recordings considered here, we observed substantial within-subject differences in the absolute values of PCI^{ST} depending on the stimulation site. These results suggest the presence of local differences in the ability of brain circuits to engage in complex patterns of causal interactions. Whether this is mainly due to the intrinsic properties of the stimulated node, or rather to the specific connectivity of the network sampled by the SEEG implantation, is an interesting question that can be addressed in future studies by adding a global measurement. In this regard, the possibility of calculating and comparing PCI^{ST} on both local field potentials and simultaneous global EEG recordings after SPES at different sites would offer a clear advantage.

Finally, mesoscale assessment of perturbational complexity is in an ideal position to link microscale explorations at the bench to the macroscale measurements performed at the bedside of brain-injured patients. This connection is fundamental as experiments in both cortical slices [27] and unresponsiveness wakefulness syndrome patients [79] suggest that the fundamental mechanism of loss of complexity is the tendency of neurons to enter a silent period upon an initial activation (OFF-period).

In conclusion, PCI^{ST}, a novel brain complexity index based on dimensionality reduction and the quantification of state transitions, may not only provide a reliable, fast and potentially online option for the assessment of consciousness in the clinical setting, but also serve as a general translational tool for exploring the mechanisms of loss and recovery of brain complexity across species, scales, and models.

Materials and methods

Participants

Healthy subjects. The benchmark dataset consisted of 382 TMS/hd-EEG sessions reported in previous works [16, 17, 79] . Data were recorded from 108 healthy subjects (female, n = 63; age range = 18–80 years) in two conditions: (1) while they were unresponsive and did not provide any subjective report upon awakening (NREM sleep, n = 19; midazolam sedation at anesthetic concentrations, n = 6; anesthesia with xenon, n = 6; anesthesia with propofol, n = 6) and (2) while they were awake and able to provide an immediate subjective report (n = 103, including 32 subjects also recorded in the previously described unresponsive conditions). The experimental protocols applied during sleep and anesthesia have been detailed elsewhere [16, 17]. In short, healthy volunteers with history or presence of major medical/neurological disorders and of drug/alcohol abuse were excluded. All participants underwent neurological screening to exclude those at risk of potential adverse effects of TMS. Protocols and informed consents were approved by the local ethical committees (Ospedale "L. Sacco" in Milan, Italy; University of Wisconsin, Madison; Medical School of the University of Liège, Belgium).

Brain-injured patients. TMS/hd-EEG data were also obtained in a population of 108 brain-injured patients (95 reported in a previous work [17]) with newly acquired data recorded following the same previously reported protocol [17]. Besides screening for potential adverse effects of TMS, exclusion criteria were medical instability, refractory generalized seizures, and history of neurodegenerative or psychiatric disease. Sixteen brain-injured patients were conscious and encompassed 5 individuals affected by locked-in syndrome (LIS) and 11 individuals who emerged from minimally conscious state (EMCS) by recovering functional communication and/or functional use of objects after a previous DOC. The remaining 92 brain-

injured patients had a severe disorder of consciousness (DOC) and were repeatedly evaluated with the Coma Recovery Scale-Revised (CRS-R) for a period of 1 week (4 times, every other day). Patients showing only reflexive behavior across all evaluations were considered as being unresponsive (Unresponsive Wakefulness Syndrome UWS, formerly known as vegetative state, 43 patients), whereas patients showing signs of nonreflexive behaviors in at least one evaluation were considered as minimally conscious (MCS, 49 patients). Protocols and informed consents were approved by the local ethical committees (Milan, Italy: Istituto di Ricovero e Cura a Carattere Scientifico Fondazione Don Gnocchi Onlus, Azienda Socio-Sanitaria Territoriale, Grande Ospedale Metropolitano Niguarda Cà Granda, and Fondazione Europea per la Ricerca Biomedica; Liège, Belgium: Medical School of the University of Liège). Written informed consent was obtained from healthy subjects, from communicative patients, and from legal surrogates of DOC patients.

Epileptic patients. Data included in the present study derived from a dataset collected during the pre-surgical evaluation of nine (eight previously reported [22]) neurosurgical patients with a history of drug-resistant, focal epilepsy. All subjects were candidates for surgical removal of the epileptic focus. During the pre-surgical evaluation all patients underwent individual investigation with SPES and simultaneous SEEG recordings for mapping eloquent areas and for precisely identifying the epileptogenic cortical network [75]. The investigated hemisphere, the duration of implantation and the location and number of stimulation sites were determined based on the non-invasive clinical assessment. The stimulation, recording and data treatment procedures were approved by the local ethical committee (Niguarda Hospital, Milan, Italy). All patients provided written informed consent.

TMS-EEG measurements and data analysis

Specific protocols for acquiring TMS/hd-EEG potentials were described in [16] and [17]. In brief, data were recorded with a 60-channel TMS-compatible EEG amplifier and MRI-guided TMS pulses were delivered with a focal biphasic stimulator. In each subject, multiple sessions of ~200 stimuli were collected with TMS targeted to different areas at different intensities accordingly to the specific protocol. Precision and reproducibility of stimulation were controlled using a Navigated Brain Stimulation (NBS) system (Nexstim Ltd., Finland). The maximum electrical field at the cortex varied within the range of 80 to 160 V/m and targets were selected based on the individual anatomical MRI from within the middle-caudal portion of the superior frontal gyrus, superior parietal gyrus, superior occipital gyrus, and the midline sensorimotor cortex. In brain-injured patients, the stimulation of targets affected by cortical lesions identified on individual magnetic resonance images was deliberately avoided because the EEG response of these areas may be absent or unreliable.

Data was analyzed as previously described [17]. EEG responses to TMS were visually inspected to reject single trials and channels with bad signal quality. Independent component analysis was applied to remove residual artifactual components resulting from eye movements and muscle activations. Bad channels were then interpolated using spherical interpolation and data were bandpass filtered (0.1-45Hz), downsampled to 725 Hz, segmented between -400 and 400ms, re-referenced to the average, baseline corrected (-400 to -5 ms) and averaged across trials.

Intra-cerebral measurements and data analysis

The procedures for SEEG data acquisition are described in [22]. Briefly, intracerebral activity was recorded from platinum–iridium semiflexible multi-contact intracerebral electrodes, with a diameter of 0.8 mm, a contact length of 2 mm, an inter-contact distance of 1.5 mm and a maximum of 18 contacts per electrode (Dixi Medical, Besancon France - Fig 1A-B). SEEG signals were recorded using a 192-channel recording system (NIHON-KOHDEN NEUROFAX-110) with a sampling rate of 1000 Hz. Data were recorded and exported in EEG Nihon-Kohden format. Recordings were referenced to a contact located entirely in the white matter. Electrical stimulation was applied through one pair of adjacent contacts (amplitude 5 mA, frequency=1 Hz, # of stimuli per session=30), while SEEG activity was simultaneously recorded from all other bipolar contacts. The stimulation, recording and data treatment procedures were approved by the local Ethical Committee (protocol number: ID 939, Niguarda Hospital, Milan, Italy). All patients provided written informed consent. SEEG data recorded during both wakefulness and NREM were imported from EEG Nihon Kohden format into Matlab and converted using a customized Matlab-based script. Data were subjected to linear detrend and bandpass filtering (0.5 – 300 Hz), using a third order Butterworth filter. Bipolar montages were calculated by subtracting the signals from adjacent contacts of the same depth-electrode to minimize common electrical noise and to maximize spatial resolution [80, 81]. Single trials were obtained by using a digital trigger simultaneous to each SPES delivery. Stimulation artifact was reduced by applying a Tukey-windowed median filtering, as in [82], between -5 and 5 ms. Finally, trials and contacts showing pathological activity [83] were detected by visual inspection excluded from the analysis.

Perturbational complexity index based on state transitions

The state transition based perturbational complexity index (PCI^{ST}) is composed of two steps: dimensionality reduction and transition quantification. In the first step, singular value decomposition (SVD) of the response is performed in order to effectively reduce the dimension of the data. More specifically, let **X** be the $N \times T$ matrix containing trial-averaged signals $x_n(t) = [x_n(t_1), \ldots, x_n(t_k), \ldots x_n(t_T)]$ of a response to a perturbation recorded from $n = 1 \ldots N$ different spatial locations and $k = 1 \ldots T$ time samples. **X** can be represented by a trajectory $\mathbf{X}(t)$ in the *N*–dimensional space spanned by the spatial locations $\mathbf{e}_n$:

$$\mathbf{X}(t) = \sum_{n=1}^{N} x_n(t)\mathbf{e}_n \tag{1}$$

Let $t = 0$ be the instant of perturbation and $\mathbf{X}_{RES}(t) = \{\mathbf{X}(t) \mid t > 0\}$ be the response signal. Then let $\mathbf{a}_n$ be the normalized eigenvectors of the autocorrelation matrix **A** calculated from the response signal,

$$\mathbf{A} = \mathbf{X}_{RES}(t) \times \mathbf{X}_{RES}(t)^T = \left\{ \sum_{t>0} x_n(t) x_m(t) \mid n, m = 1 \ldots N \right\} \tag{2}$$

In the new orthogonal basis, $\{\mathbf{a}_n\}$, **X** can be represented by a rotated trajectory $\mathbf{Y}(t)$:

$$\mathbf{Y}(t) = \sum_{n=1}^{N} y_n(t)\mathbf{a}_n = \sum_{n,m=1}^{N} x_m(t)(\mathbf{a}_n \cdot \mathbf{e}_m)\mathbf{a}_n \tag{3}$$

The $N \times T$ matrix **Y** is thus composed by projecting the data **X** in the space spanned by the principal components (PC) obtained from SVD of the response signal. The PCs are then selected in terms of the eigenvalues of **A** sorted in decreasing order, so as to account for at least 99% of the response strength measured in terms of the square mean field power, $\sum_{n,k} |y_n(t_k)|^2$.

Next, components with low signal-to-noise ratio (SNR ≤ 1.1) are removed, and the remaining N_C responsive principal components are used for transition quantification in the following (Fig 2A).

As the resulting components are linearly independent, we regard each component $y_n(t)$ separately and consider its time-delayed embedded form given by:

$$\mathbf{y}_n(t) = \left[y_n(t), y_n(t-\tau), \ldots, y_n(t-L\times\tau) \right] \tag{4}$$

where L and τ are the dimension and the delay of the embedding, respectively and $n = 1 \ldots N_C$. Given an embedded time-series $\mathbf{y}_n(t)$, its distance matrix $\mathbf{D}_n$ is then defined as the Euclidean distance between all timepoints of the signal (Fig 2B):

$$\mathbf{D}_n(t_i, t_j) = \left\| \mathbf{y}_n(t_i) - \mathbf{y}_n(t_j) \right\| \tag{5}$$

Both matrices are then thresholded at several scales (Fig 2C): for each threshold ε we calculate the transition matrix defined as the contour plot of the correspondent distance matrix at the scale ε (Fig 2D):

$$\mathbf{T}_n(\varepsilon, t_i, t_j) = \begin{cases} 1, & if\ \mathbf{D}_n(t_i, t_j) = \varepsilon \\ 0, & otherwise \end{cases} \tag{6}$$

The transition matrix can be thought as the unidirectional derivative of the recurrence matrix $\mathbf{R}_n$, also known as recurrence plot [56]:

$$\mathbf{R}_n(\varepsilon, t_i, t_j) = \begin{cases} 1, & if\ \mathbf{D}_n(t_i, t_j) < \varepsilon \\ 0, & otherwise \end{cases} \tag{7}$$

Transition matrices can thus be interpreted as measuring not recurrent states, but transitions between states – between recurrent states, $\mathbf{R}_n(\varepsilon, t_i, t_j)=1$, and non-recurrent states, $\mathbf{R}_n(\varepsilon, t_i, t_j)=0$.

Next, we simply cumulate the transition matrix across T_C time samples and calculate the mean number of state transitions (NST) for a component n at a given threshold ε as

$$\mathrm{NST}_n(\varepsilon) = \frac{1}{{T_C}^2} \sum_{i=1}^{T_C} \sum_{j=1}^{T_C} \mathbf{T}_n(\varepsilon, t_i, t_j) \tag{8}$$

The NST quantifies the average amount of state transitions in a time-series at a given scale ε. Transitions are averaged separately for both $T_C = T_B$ baseline samples (t<0), NST_n^{base} and $T_C = T_R$ response samples (t>0), NST_n^{res}.

The threshold ε represents a crucial amplitude scale through which information is encoded in the signal in terms of distance crossings. For very small scales (threshold ε' in Fig 2D), most transitions occur in the baseline and the structures appearing in the Transition matrices at these scales are likely not caused by the perturbation. By increasing the value of ε, transitions start to appear mostly in the response to the stimulus and are, therefore, likely due to the perturbation. Thus, in order to measure the amount of temporal information encoded in the response over and above the amount encoded in the baseline, we search for the scale in which the weighted difference between NST_n^{res} and NST_n^{bases} is maximized (threshold ε^* in Fig 2D):

$$\varepsilon_n^* = \arg\max \left[\mathrm{NST}_n^{res}(\varepsilon) - k \times \mathrm{NST}_n^{base}(\varepsilon) \right] \tag{9}$$

The parameter k is introduced to control the relative weight between pre and post-stimulus state transitions. By setting the value of k, the crucial scale ε_n^* becomes a data-driven parameter determined by the pre-post comparison for each principal component. Therefore, the temporal complexity of the nth component ($\Delta\mathrm{NST}_n$) is the maximized weighted difference at the optimal scale ε_n^* scaled by the number of response samples (T_R) (Fig 2E). The scaling factor yields a quantity that is extensive with the length of the signal's response and largely independent on the sampling rate (Fig 5):

$$\Delta\mathrm{NST}_n = T_R \left[\mathrm{NST}_n^{res}(\varepsilon_n^*) - k \times \mathrm{NST}_n^{base}(\varepsilon_n^*) \right] \tag{10}$$

Finally, the State Transitions Perturbational Complexity Index is defined as the sum of the temporal complexity measured by ΔNST_n taken across all the N_C selected principal components of the signal:

$$PCI^{ST} = \sum_{n=1}^{N_C} \Delta NST_n \quad (11)$$

Calculating PCIST

PCIST was calculated on TMS/EEG signals and SPES/SEEG recordings. In both cases, a crucial step in calculating PCIST is to control for stationary baseline-like activations that are likely not caused by the perturbation. This is done in two ways: (i) by removing principal components with low signal-to-noise ratio and (ii) by comparing between pre and post-stimulus transitions in the remaining components and selecting an amplitude scale that maximizes the information content of the response, over and above the content of the baseline. In this work, minimum SNR of the components accounting for 99% of the response strength was set to 1.1 and the k parameter controlling the relative weight between pre and post-stimulus state transitions in the remaining components was set to 1.2, value at which there is maximum separation between conscious and unconscious conditions (see S4 Fig). Since results were largely independent on the delay and embedding dimension (S4 Fig), distance matrices of the principal components were calculated for the simplest case of L = 1.

PCIST was calculated on TMS/EEG signals using three different EEG setups: hd-EEG (all 60 channels), 10-20 system (channels numbered 1, 2, 3, 7, 9, 11, 13, 19, 25, 27, 29, 31, 33, 45, 47, 49, 51, 53, 57, 59) and a reduced setup with 8 channels (numbered 9, 11, 27, 29, 31, 49, 57, 59). For each setup, signals were referenced to the corresponding common average reference.

Finally the baseline and response interval were respectively defined as (-400ms, -50ms) and (0ms, 300ms) for TMS/EEG sessions [16, 17], and as (-250ms, -50ms) and (10ms, 600ms) for SPES/SEEG sessions [22] – 0ms being the onset of the stimulation.

Statistical analysis

Statistical analysis was performed with IBM SPSS v.22.0. Data are presented as mean ± standard deviation (SD), and p-values less than 0.01 were considered significant. Normality of data was checked with the Shapiro-Wilk test and nonparametric testing was employed if data were not normally distributed. Wilcoxon-ranksum test was used for evaluating the discrimination between conscious and unconscious conditions as well as average effects of sampling frequency on the absolute value of PCI^{ST}. Univariate ANOVA for repeated measurements followed by Bonferroni post hoc test was used for testing the effects of number of channels and trials.

A linear support vector classifier [38], independently trained on all TMS/EEG sessions of the benchmark dataset, was employed to predict the level of consciousness of brain-injured patients who had recovered from coma (see S2 Fig for computational details). The classification power of discriminating different levels of consciousness was quantified by the area under the receiver operating characteristic curve (AUC). The Fisher's Discriminant Ratio (FDR) – calculated as the square of the difference between the means of the distributions divided by the sum of their variances – was used as a class separability criterion between conscious and unconscious conditions.

Acknowledgments

We thank Nestor Caticha, Anna Cattani, Thierry Nieus, Simone Russo and Angela Comanducci for useful discussions during the course of this work. We thank Sasha D'Ambrosio for help with data collection and analysis.

Funding

This work was supported by São Paulo Research Foundation (FAPESP), grants 2016/08263-9 (AGC) and 2017/03678-9 (RC) and by the European Union's Horizon 2020 Framework Programme for Research and Innovation, grants 785907-Human Brain Project SGA2, 720270-Human Brain Project SGA1 and EU Project LUMINOUS H2020-FETOPEN-2014-2015-RIA G.A. n. 686764 (MM). The study has also been partially funded by the Belgian National Funds for Scientific Research FRS-FNRS (OG); the James McDonnell Foundation Scholar Award 2013 (MM); Wallonie-Bruxelles International and International Foundation for Clinical Neurophysiology (OB); the Mind Science Foundation; the BIAL foundation; the Public Utility Foundation Université Européenne du Travail. The funders had no role in study design, data collection and analysis, decision to publish, or preparation of the manuscript.

References

1. Bassett DS, Bullmore ET. Human brain networks in health and disease. Current opinion in neurology. 2009;22(4):340-7. doi: 10.1097/WCO.0b013e32832d93dd. PubMed PMID: 19494774; PubMed Central PMCID: PMC2902726.
2. Deco G, Tononi G, Boly M, Kringelbach ML. Rethinking segregation and integration: contributions of whole-brain modelling. Nature reviews Neuroscience. 2015;16(7):430-9. doi: 10.1038/nrn3963. PubMed PMID: 26081790.
3. Seth AK, Barrett AB, Barnett L. Causal density and integrated information as measures of conscious level. Philosophical transactions Series A, Mathematical, physical, and engineering sciences. 2011;369(1952):3748-67. doi: 10.1098/rsta.2011.0079. PubMed PMID: 21893526.

4. Sporns O, Tononi G, Edelman GM. Connectivity and complexity: the relationship between neuroanatomy and brain dynamics. Neural networks : the official journal of the International Neural Network Society. 2000;13(8-9):909-22. PubMed PMID: 11156201.
5. Tononi G, Boly M, Massimini M, Koch C. Integrated information theory: from consciousness to its physical substrate. Nature reviews Neuroscience. 2016;17(7):450-61. doi: 10.1038/nrn.2016.44. PubMed PMID: 27225071.
6. Tononi G, Edelman GM. Consciousness and complexity. Science. 1998;282(5395):1846-51. PubMed PMID: 9836628.
7. Barrett AB, Murphy M, Bruno MA, Noirhomme Q, Boly M, Laureys S, et al. Granger causality analysis of steady-state electroencephalographic signals during propofol-induced anaesthesia. PloS one. 2012;7(1):e29072. doi: 10.1371/journal.pone.0029072. PubMed PMID: 22242156; PubMed Central PMCID: PMC3252303.
8. Jobst BM, Hindriks R, Laufs H, Tagliazucchi E, Hahn G, Ponce-Alvarez A, et al. Increased Stability and Breakdown of Brain Effective Connectivity During Slow-Wave Sleep: Mechanistic Insights from Whole-Brain Computational Modelling. Scientific reports. 2017;7(1):4634. doi: 10.1038/s41598-017-04522-x. PubMed PMID: 28680119; PubMed Central PMCID: PMC5498661.
9. Schartner M, Seth A, Noirhomme Q, Boly M, Bruno MA, Laureys S, et al. Complexity of Multi-Dimensional Spontaneous EEG Decreases during Propofol Induced General Anaesthesia. PloS one. 2015;10(8):e0133532. doi: 10.1371/journal.pone.0133532. PubMed PMID: 26252378; PubMed Central PMCID: PMC4529106.
10. Solovey G, Alonso LM, Yanagawa T, Fujii N, Magnasco MO, Cecchi GA, et al. Loss of Consciousness Is Associated with Stabilization of Cortical Activity. The Journal of neuroscience : the official journal of the Society for Neuroscience. 2015;35(30):10866-77. doi: 10.1523/JNEUROSCI.4895-14.2015. PubMed PMID: 26224868; PubMed Central PMCID: PMC4518057.
11. Chennu S, Annen J, Wannez S, Thibaut A, Chatelle C, Cassol H, et al. Brain networks predict metabolism, diagnosis and prognosis at the bedside in disorders of consciousness. Brain : a journal of neurology. 2017;140(8):2120-32. doi: 10.1093/brain/awx163. PubMed PMID: 28666351.
12. Gosseries O, Schnakers C, Ledoux D, Vanhaudenhuyse A, Bruno MA, Demertzi A, et al. Automated EEG entropy measurements in coma, vegetative state/unresponsive wakefulness syndrome and minimally conscious state. Functional neurology. 2011;26(1):25-30. PubMed PMID: 21693085; PubMed Central PMCID: PMC3814509.
13. Rosanova M, Gosseries O, Casarotto S, Boly M, Casali AG, Bruno MA, et al. Recovery of cortical effective connectivity and recovery of consciousness in vegetative patients. Brain : a journal of neurology. 2012;135(Pt 4):1308-20. doi: 10.1093/brain/awr340. PubMed PMID: 22226806; PubMed Central PMCID: PMC3326248.
14. Sitt JD, King JR, El Karoui I, Rohaut B, Faugeras F, Gramfort A, et al. Large scale screening of neural signatures of consciousness in patients in a vegetative or minimally conscious state. Brain : a journal of neurology. 2014;137(Pt 8):2258-70. doi: 10.1093/brain/awu141. PubMed PMID: 24919971; PubMed Central PMCID: PMC4610185.
15. Thul A, Lechinger J, Donis J, Michitsch G, Pichler G, Kochs EF, et al. EEG entropy measures indicate decrease of cortical information processing in Disorders of Consciousness. Clinical neurophysiology : official journal of the International Federation of Clinical Neurophysiology. 2016;127(2):1419-27. doi: 10.1016/j.clinph.2015.07.039. PubMed PMID: 26480834.
16. Casali AG, Gosseries O, Rosanova M, Boly M, Sarasso S, Casali KR, et al. A theoretically based index of consciousness independent of sensory processing and behavior. Science translational medicine. 2013;5(198):198ra05. doi: 10.1126/scitranslmed.3006294. PubMed PMID: 23946194.

17. Casarotto S, Comanducci A, Rosanova M, Sarasso S, Fecchio M, Napolitani M, et al. Stratification of unresponsive patients by an independently validated index of brain complexity. Annals of neurology. 2016;80(5):718-29. doi: 10.1002/ana.24779. PubMed PMID: 27717082; PubMed Central PMCID: PMC5132045.
18. Sarasso S, Boly M, Napolitani M, Gosseries O, Charland-Verville V, Casarotto S, et al. Consciousness and Complexity during Unresponsiveness Induced by Propofol, Xenon, and Ketamine. Current biology : CB. 2015;25(23):3099-105. doi: 10.1016/j.cub.2015.10.014. PubMed PMID: 26752078.
19. Hallez H, Vanrumste B, Grech R, Muscat J, De Clercq W, Vergult A, et al. Review on solving the forward problem in EEG source analysis. Journal of neuroengineering and rehabilitation. 2007;4:46. doi: 10.1186/1743-0003-4-46. PubMed PMID: 18053144; PubMed Central PMCID: PMC2234413.
20. Baillet SM, J. C.; Leahy, R. M.;. Electromagnetic Brain Mapping. IEEE Signal Processing Magazine. 2001;(November):14-30. doi: 10.1109/79.962275.
21. Lewis LD, Weiner VS, Mukamel EA, Donoghue JA, Eskandar EN, Madsen JR, et al. Rapid fragmentation of neuronal networks at the onset of propofol-induced unconsciousness. Proceedings of the National Academy of Sciences of the United States of America. 2012;109(49):E3377-86. doi: 10.1073/pnas.1210907109. PubMed PMID: 23129622; PubMed Central PMCID: PMC3523833.
22. Pigorini A, Sarasso S, Proserpio P, Szymanski C, Arnulfo G, Casarotto S, et al. Bistability breaks-off deterministic responses to intracortical stimulation during non-REM sleep. NeuroImage. 2015;112:105-13. doi: 10.1016/j.neuroimage.2015.02.056. PubMed PMID: 25747918.
23. Bettinardi RG, Tort-Colet N, Ruiz-Mejias M, Sanchez-Vives MV, Deco G. Gradual emergence of spontaneous correlated brain activity during fading of general anesthesia in rats: Evidences from fMRI and local field potentials. NeuroImage. 2015;114:185-98. doi: 10.1016/j.neuroimage.2015.03.037. PubMed PMID: 25804643; PubMed Central PMCID: PMC4461308.
24. Olcese U, Bos JJ, Vinck M, Lankelma JV, van Mourik-Donga LB, Schlumm F, et al. Spike-Based Functional Connectivity in Cerebral Cortex and Hippocampus: Loss of Global Connectivity Is Coupled to Preservation of Local Connectivity During Non-REM Sleep. The Journal of neuroscience : the official journal of the Society for Neuroscience. 2016;36(29):7676-92. doi: 10.1523/JNEUROSCI.4201-15.2016. PubMed PMID: 27445145.
25. Vyazovskiy VV, Faraguna U, Cirelli C, Tononi G. Triggering slow waves during NREM sleep in the rat by intracortical electrical stimulation: effects of sleep/wake history and background activity. Journal of neurophysiology. 2009;101(4):1921-31. doi: 10.1152/jn.91157.2008. PubMed PMID: 19164101; PubMed Central PMCID: PMC2695630.
26. Vyazovskiy VV, Olcese U, Cirelli C, Tononi G. Prolonged wakefulness alters neuronal responsiveness to local electrical stimulation of the neocortex in awake rats. Journal of sleep research. 2013;22(3):239-50. doi: 10.1111/jsr.12009. PubMed PMID: 23607417; PubMed Central PMCID: PMC3723708.
27. D'Andola M, Rebollo B, Casali AG, Weinert JF, Pigorini A, Villa R, et al. Bistability, Causality, and Complexity in Cortical Networks: An In Vitro Perturbational Study. Cerebral cortex. 2017:1-10. doi: 10.1093/cercor/bhx122. PubMed PMID: 28525544.
28. Sanchez-Vives MV, Massimini M, Mattia M. Shaping the Default Activity Pattern of the Cortical Network. Neuron. 2017;94(5):993-1001. doi: 10.1016/j.neuron.2017.05.015. PubMed PMID: 28595056.
29. Storm JF, Boly M, Casali AG, Massimini M, Olcese U, Pennartz CMA, et al. Consciousness Regained: Disentangling Mechanisms, Brain Systems, and Behavioral Responses. The Journal of neuroscience : the official journal of the Society for Neuroscience.

2017;37(45):10882-93. doi: 10.1523/JNEUROSCI.1838-17.2017. PubMed PMID: 29118218; PubMed Central PMCID: PMC5678021.
30. Axmacher N, Henseler MM, Jensen O, Weinreich I, Elger CE, Fell J. Cross-frequency coupling supports multi-item working memory in the human hippocampus. Proceedings of the National Academy of Sciences of the United States of America. 2010;107(7):3228-33. doi: 10.1073/pnas.0911531107. PubMed PMID: 20133762; PubMed Central PMCID: PMC2840289.
31. Bragin A, Jando G, Nadasdy Z, Hetke J, Wise K, Buzsaki G. Gamma (40-100 Hz) oscillation in the hippocampus of the behaving rat. The Journal of neuroscience : the official journal of the Society for Neuroscience. 1995;15(1 Pt 1):47-60. PubMed PMID: 7823151.
32. Canolty RT, Edwards E, Dalal SS, Soltani M, Nagarajan SS, Kirsch HE, et al. High gamma power is phase-locked to theta oscillations in human neocortex. Science. 2006;313(5793):1626-8. doi: 10.1126/science.1128115. PubMed PMID: 16973878; PubMed Central PMCID: PMC2628289.
33. Lisman JE, Jensen O. The theta-gamma neural code. Neuron. 2013;77(6):1002-16. doi: 10.1016/j.neuron.2013.03.007. PubMed PMID: 23522038; PubMed Central PMCID: PMC3648857.
34. Young CK, Eggermont JJ. Coupling of mesoscopic brain oscillations: recent advances in analytical and theoretical perspectives. Progress in neurobiology. 2009;89(1):61-78. doi: 10.1016/j.pneurobio.2009.06.002. PubMed PMID: 19549556.
35. Mutanen T, Nieminen JO, Ilmoniemi RJ. TMS-evoked changes in brain-state dynamics quantified by using EEG data. Frontiers in human neuroscience. 2013;7:155. doi: 10.3389/fnhum.2013.00155. PubMed PMID: 23630486; PubMed Central PMCID: PMC3635036.
36. Marwan N, Carmen Romano M, Thiel M, Kurths J. Recurrence plots for the analysis of complex systems. Physics Reports. 2007;438:237-329.
37. Webber CL, Jr., Zbilut JP. Dynamical assessment of physiological systems and states using recurrence plot strategies. Journal of applied physiology. 1994;76(2):965-73. doi: 10.1152/jappl.1994.76.2.965. PubMed PMID: 8175612.
38. Pedregosa F, Varoquaux G, Gramfort A, Michel V, Thirion B, Grisel O. Scikit-learn: machine learning in python. J Mach Learn Res. 2011;12:2825-30.
39. Massimini M, Boly M, Casali A, Rosanova M, Tononi G. A perturbational approach for evaluating the brain's capacity for consciousness. Progress in brain research. 2009;177:201-14. doi: 10.1016/S0079-6123(09)17714-2. PubMed PMID: 19818903.
40. Paus T. Inferring causality in brain images: a perturbation approach. Philosophical transactions of the Royal Society of London Series B, Biological sciences. 2005;360(1457):1109-14. doi: 10.1098/rstb.2005.1652. PubMed PMID: 16087451; PubMed Central PMCID: PMC1854935.
41. Wackermann J. Beyond mapping: estimating complexity of multichannel EEG recordings. Acta neurobiologiae experimentalis. 1996;56(1):197-208. PubMed PMID: 8787174.
42. Lehmann D. Principles of spatial analysis. In: Gevins ASR, A., editor. Methods of analysis of brain electrical and magnetic signals. EEG Handbook (revised series). I. Amsterdam: Elsevier; 1987. p. 309-54.
43. Kayser J, Fong R, Tenke CE, Bruder GE. Event-related brain potentials during auditory and visual word recognition memory tasks. Brain research Cognitive brain research. 2003;16(1):11-25. PubMed PMID: 12589884.
44. Kayser J, Tenke CE. Principal components analysis of Laplacian waveforms as a generic method for identifying ERP generator patterns: I. Evaluation with auditory oddball tasks. Clinical neurophysiology : official journal of the International Federation of Clinical Neurophysiology. 2006;117(2):348-68. doi: 10.1016/j.clinph.2005.08.034. PubMed PMID: 16356767.
45. Pourtois G, Delplanque S, Michel C, Vuilleumier P. Beyond conventional event-related brain potential (ERP): exploring the time-course of visual emotion processing using topographic

and principal component analyses. Brain topography. 2008;20(4):265-77. doi: 10.1007/s10548-008-0053-6. PubMed PMID: 18338243.
46. Skrandies W, Lehmann D. Spatial principal components of multichannel maps evoked by lateral visual half-field stimuli. Electroencephalography and clinical neurophysiology. 1982;54(6):662-7. PubMed PMID: 6183099.
47. Spencer KM, Dien J, Donchin E. A componential analysis of the ERP elicited by novel events using a dense electrode array. Psychophysiology. 1999;36(3):409-14. PubMed PMID: 10352565.
48. Spencer KM, Dien J, Donchin E. Spatiotemporal analysis of the late ERP responses to deviant stimuli. Psychophysiology. 2001;38(2):343-58. PubMed PMID: 11347879.
49. Suter CM. Principal component analysis of average evoked potentials. Experimental neurology. 1970;29(2):317-27. PubMed PMID: 5504473.
50. Duffy FH, Jones K, Bartels P, McAnulty G, Albert M. Unrestricted principal components analysis of brain electrical activity: issues of data dimensionality, artifact, and utility. Brain topography. 1992;4(4):291-307. PubMed PMID: 1510873.
51. Jensen O, Gips B, Bergmann TO, Bonnefond M. Temporal coding organized by coupled alpha and gamma oscillations prioritize visual processing. Trends in neurosciences. 2014;37(7):357-69. doi: 10.1016/j.tins.2014.04.001. PubMed PMID: 24836381.
52. Canolty RT, Knight RT. The functional role of cross-frequency coupling. Trends in cognitive sciences. 2010;14(11):506-15. doi: 10.1016/j.tics.2010.09.001. PubMed PMID: 20932795; PubMed Central PMCID: PMC3359652.
53. Fell J, Axmacher N. The role of phase synchronization in memory processes. Nature reviews Neuroscience. 2011;12(2):105-18. doi: 10.1038/nrn2979. PubMed PMID: 21248789.
54. Florin E, Baillet S. The brain's resting-state activity is shaped by synchronized cross-frequency coupling of neural oscillations. NeuroImage. 2015;111:26-35. doi: 10.1016/j.neuroimage.2015.01.054. PubMed PMID: 25680519; PubMed Central PMCID: PMC4387013.
55. Jensen O, Colgin LL. Cross-frequency coupling between neuronal oscillations. Trends in cognitive sciences. 2007;11(7):267-9. doi: 10.1016/j.tics.2007.05.003. PubMed PMID: 17548233.
56. Eckmann J-P, Kamphorst SP, Ruelle D. Recurrence plots of dynamical systems. Europhysics Letters. 1987;5:973-7.
57. Poincarè J. Sur le probléme des trois corps et les équations de la dynamic. Acta Math. 1890;13:1-270.
58. Eroglu D, Peron TK, Marwan N, Rodrigues FA, Costa Lda F, Sebek M, et al. Entropy of weighted recurrence plots. Physical review E, Statistical, nonlinear, and soft matter physics. 2014;90(4):042919. doi: 10.1103/PhysRevE.90.042919. PubMed PMID: 25375579.
59. Gao J. Recurrence Time Statistics for Chaotic Systems and Their Applications. Physical Review Letters. 1999;83(16):3178-81.
60. Gao J, Hu J. Fast monitoring of epileptic seizures using recurrence time statistics of electroencephalography. Frontiers in computational neuroscience. 2013;7:122. doi: 10.3389/fncom.2013.00122. PubMed PMID: 24137126; PubMed Central PMCID: PMC3794444.
61. Marwan N, Wessel N, Meyerfeldt U, Schirdewan A, Kurths J. Recurrence-plot-based measures of complexity and their application to heart-rate-variability data. Physical review E, Statistical, nonlinear, and soft matter physics. 2002;66(2 Pt 2):026702. doi: 10.1103/PhysRevE.66.026702. PubMed PMID: 12241313.
62. Mocenni C, Facchini A, Vicino A. Identifying the dynamics of complex spatio-temporal systems by spatial recurrence properties. Proceedings of the National Academy of Sciences of the United States of America. 2010;107(18):8097-102. doi: 10.1073/pnas.0910414107. PubMed PMID: 20404202; PubMed Central PMCID: PMC2889534.

63. Trulla L, Giuliania J, Zbilut JP, Webber C. Recurrence quantification analysis of the logistic equation with transients. Physics Letters A. 1996;223:225-60.
64. Takens F. Detecting strange attractors in turbulence. In: Springer, editor. Dynamical Systems and Turbulence. Heidelberg1981. p. 366-81.
65. Iwanski JS, Bradley E. Recurrence plots of experimental data: To embed or not to embed? Chaos. 1998;8(4):861-71. doi: 10.1063/1.166372. PubMed PMID: 12779793.
66. Little MA, McSharry PE, Roberts SJ, Costello DA, Moroz IM. Exploiting nonlinear recurrence and fractal scaling properties for voice disorder detection. Biomedical engineering online. 2007;6:23. doi: 10.1186/1475-925X-6-23. PubMed PMID: 17594480; PubMed Central PMCID: PMC1913514.
67. Baptista MSN, E. J.; Pinto, P. R. F.; Brito, M.; Kurths, J. Kolmogorov-Sinai entropy for recurrence times. Physics Letters A. 2010;374:1135-40.
68. Friston KJ. The labile brain. II. Transients, complexity and selection. Philosophical transactions of the Royal Society of London Series B, Biological sciences. 2000;355(1394):237-52. doi: 10.1098/rstb.2000.0561. PubMed PMID: 10724458; PubMed Central PMCID: PMC1692732.
69. Holzfuss J. Prediction of long-term dynamics from transients. Physical review E, Statistical, nonlinear, and soft matter physics. 2005;71(1 Pt 2):016214. doi: 10.1103/PhysRevE.71.016214. PubMed PMID: 15697705.
70. Kunze T, Hunold A, Haueisen J, Jirsa V, Spiegler A. Transcranial direct current stimulation changes resting state functional connectivity: A large-scale brain network modeling study. NeuroImage. 2016;140:174-87. doi: 10.1016/j.neuroimage.2016.02.015. PubMed PMID: 26883068.
71. Spiegler A, Kiebel SJ, Atay FM, Knosche TR. Bifurcation analysis of neural mass models: Impact of extrinsic inputs and dendritic time constants. NeuroImage. 2010;52(3):1041-58. doi: 10.1016/j.neuroimage.2009.12.081. PubMed PMID: 20045068.
72. Matsumoto R, Nair DR, LaPresto E, Bingaman W, Shibasaki H, Luders HO. Functional connectivity in human cortical motor system: a cortico-cortical evoked potential study. Brain : a journal of neurology. 2007;130(Pt 1):181-97. doi: 10.1093/brain/awl257. PubMed PMID: 17046857.
73. Buzsaki G, Anastassiou CA, Koch C. The origin of extracellular fields and currents--EEG, ECoG, LFP and spikes. Nature reviews Neuroscience. 2012;13(6):407-20. doi: 10.1038/nrn3241. PubMed PMID: 22595786; PubMed Central PMCID: PMC4907333.
74. Linden H, Tetzlaff T, Potjans TC, Pettersen KH, Grun S, Diesmann M, et al. Modeling the spatial reach of the LFP. Neuron. 2011;72(5):859-72. doi: 10.1016/j.neuron.2011.11.006. PubMed PMID: 22153380.
75. Cossu M, Cardinale F, Castana L, Citterio A, Francione S, Tassi L, et al. Stereoelectroencephalography in the presurgical evaluation of focal epilepsy: a retrospective analysis of 215 procedures. Neurosurgery. 2005;57(4):706-18; discussion -18. PubMed PMID: 16239883.
76. Nikouline V, Ruohonen J, Ilmoniemi RJ. The role of the coil click in TMS assessed with simultaneous EEG. Clinical neurophysiology : official journal of the International Federation of Clinical Neurophysiology. 1999;110(8):1325-8. PubMed PMID: 10454266.
77. Gordon PC, Desideri D, Belardinelli P, Zrenner C, Ziemann U. Comparison of cortical EEG responses to realistic sham versus real TMS of human motor cortex. Brain Stimul (in press); https://doiorg/101016/jbrs201808003. 2018. doi: 10.1016/j.brs.2018.08.003. PubMed PMID: 30143417.
78. Gosseries O, Sarasso S, Casarotto S, Boly M, Schnakers C, Napolitani M, et al. On the cerebral origin of EEG responses to TMS: insights from severe cortical lesions. Brain stimulation. 2015;8(1):142-9. doi: 10.1016/j.brs.2014.10.008. PubMed PMID: 25481074.

79. Rosanova M, Fecchio M, Casarotto S, Sarasso S, Casali AG, Pigorini A, et al. Sleep-like bistability, loss of causality and complexity in the brain of Unresponsive Wakefulness Syndrome patients. Nature Communications (in press); Bioarxiv 242644; https://doiorg/101101/242644 2018.
80. Cash SS, Halgren E, Dehghani N, Rossetti AO, Thesen T, Wang C, et al. The human K-complex represents an isolated cortical down-state. Science. 2009;324(5930):1084-7. doi: 10.1126/science.1169626. PubMed PMID: 19461004; PubMed Central PMCID: PMC3715654.
81. Gaillard R, Dehaene S, Adam C, Clemenceau S, Hasboun D, Baulac M, et al. Converging intracranial markers of conscious access. PLoS biology. 2009;7(3):e61. doi: 10.1371/journal.pbio.1000061. PubMed PMID: 19296722; PubMed Central PMCID: PMC2656551.
82. Chang JY, Pigorini A, Massimini M, Tononi G, Nobili L, Van Veen BD. Multivariate autoregressive models with exogenous inputs for intracerebral responses to direct electrical stimulation of the human brain. Frontiers in human neuroscience. 2012;6:317. doi: 10.3389/fnhum.2012.00317. PubMed PMID: 23226122; PubMed Central PMCID: PMC3510687.
83. Valentin A, Anderson M, Alarcon G, Seoane JJ, Selway R, Binnie CD, et al. Responses to single pulse electrical stimulation identify epileptogenesis in the human brain in vivo. Brain : a journal of neurology. 2002;125(Pt 8):1709-18. PubMed PMID: 12135963.

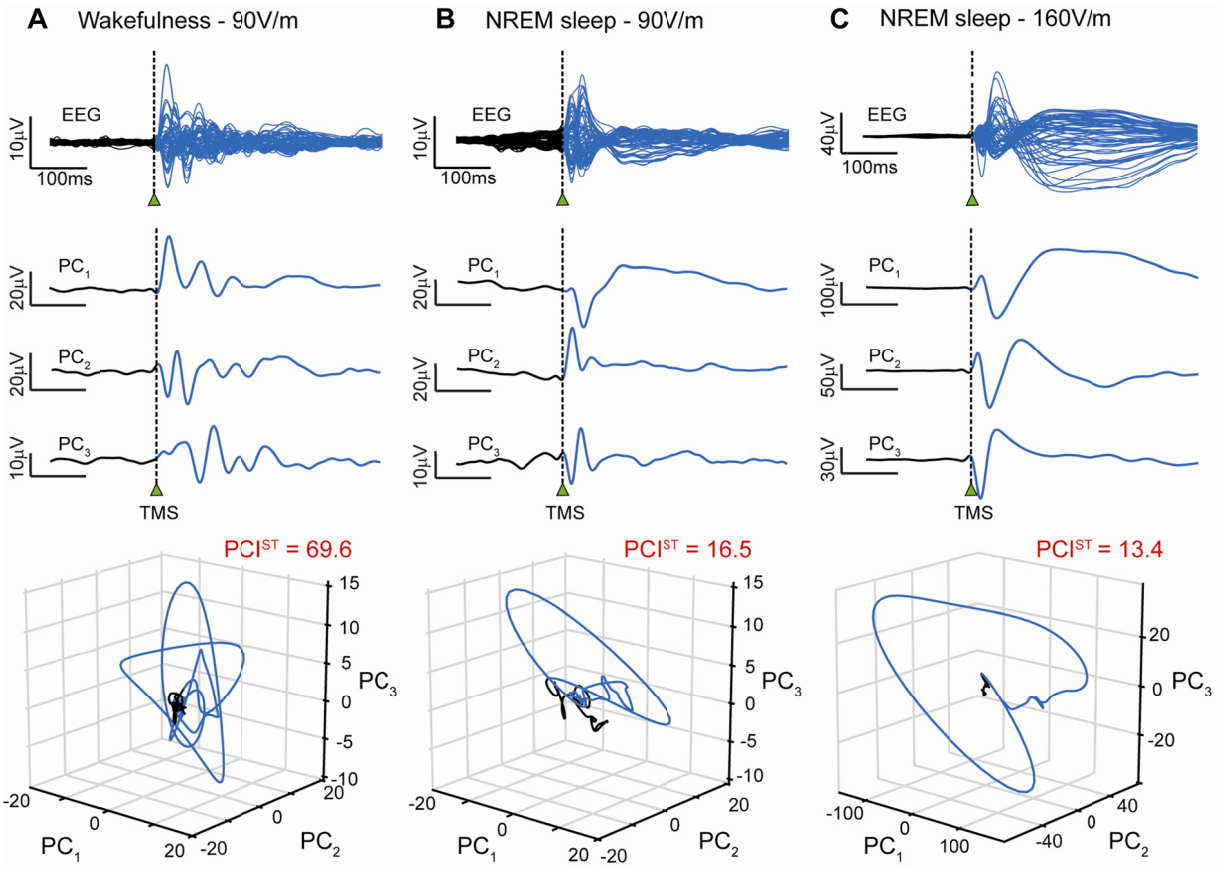

Fig 1. The spatiotemporal complexity of TMS-evoked potentials can be captured in the trajectories spanned in the principal components space. From top to bottom: TMS/EEG evoked signal displayed as a butterfly plot of the 60-channels; plot of the first three principal components (PC) ordered by eigenvalue; trajectory in the principal component space with corresponding PCI^{ST} value. Data are shown for three TMS/hd-EEG sessions with the coil target to the sensory-motor area at different intensities and during (A) alert wakefulness (stimulus at an intensity of 90V/m), (B) NREM sleep (stimulus at an intensity of 90V/m) and (C) NREM sleep (stimulus at an intensity of 160V/m). Pre-stimulus signals are shown in black, blue traces depict the TMS-evoked responses.

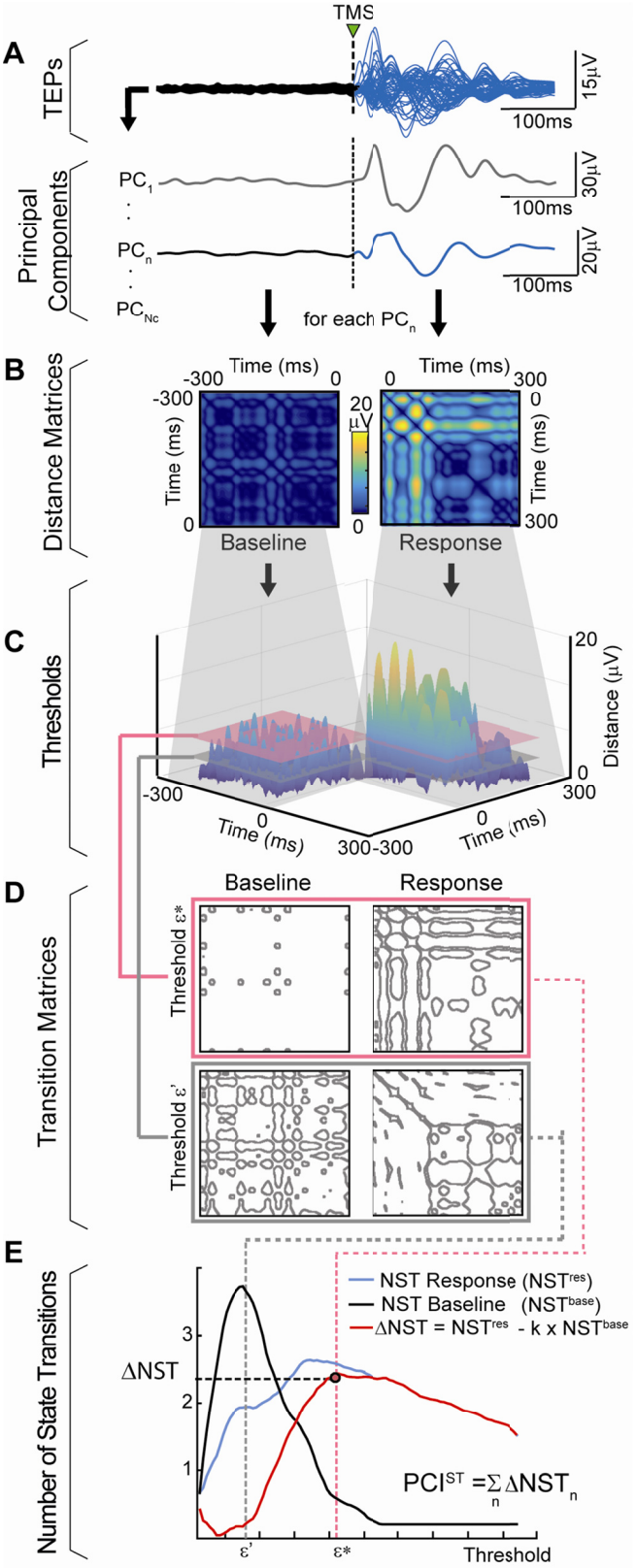

Fig 2. Calculating the Perturbational complexity index based on state transitions (PCI^{ST}) from TMS/hd-EEG evoked potentials (TEP). PCI^{ST} is calculated by performing several steps: A) TEPs (butterfly plot, top) are decomposed in N_C principal components (PC) based on the singular value decomposition of the response to the perturbation. B) For each single component (PC_n, highlighted) amplitude distances are calculated between every baseline samples (black trace in A) and between every response sample (blue trace in A), resulting in a baseline and a response distance matrix, respectively. C) These matrices are then thresholded at several scales. Two scale values are depicted in the figure: a lower threshold (ε') and a higher threshold (ε*). D) At each scale, the corresponding transition matrices are computed for both baseline and response. These matrices are used to calculate the average number of state transitions (NST) in the baseline NST^{base} and in the response NST^{res} (see Methods for further details). E) The complexity of the selected component is defined as the maximum weighted difference between the number of state transitions in the response and in the baseline (ΔNST_n). The final measure PCI^{ST} is calculated by summing the ΔNST_n values across all N_C principal components.

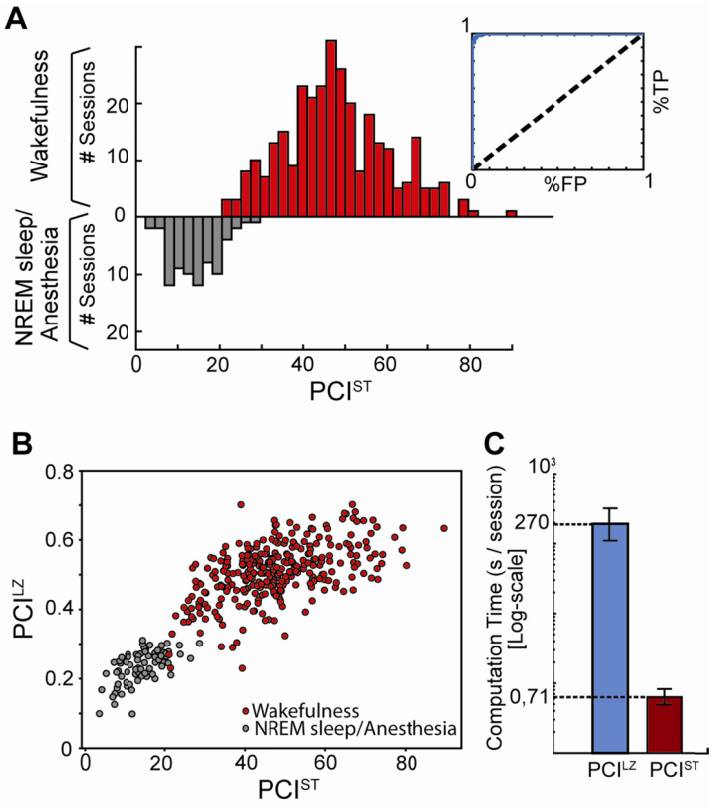

Fig 3. PCIST discriminates between consciousness and unconsciousness in healthy individuals and is faster than PCI^{LZ}. (A) Histogram of PCIST values (left) for all 382 TMS sessions obtained from 108 healthy individuals in the conscious condition (alert wakefulness, red) and unconscious condition (NREM sleep and anesthesia, grey), with the corresponding ROC curve of the distributions (right). (B) Correlation between PCIST and PCI^{LZ} values in the benchmark dataset for conscious (red) and unconscious (grey) conditions ($r=0.82$, $p<10^{-95}$). (C) Mean computation time per TMS/hd-EEG session for PCIST (red) and PCI^{LZ} (blue) calculated on the benchmark dataset.

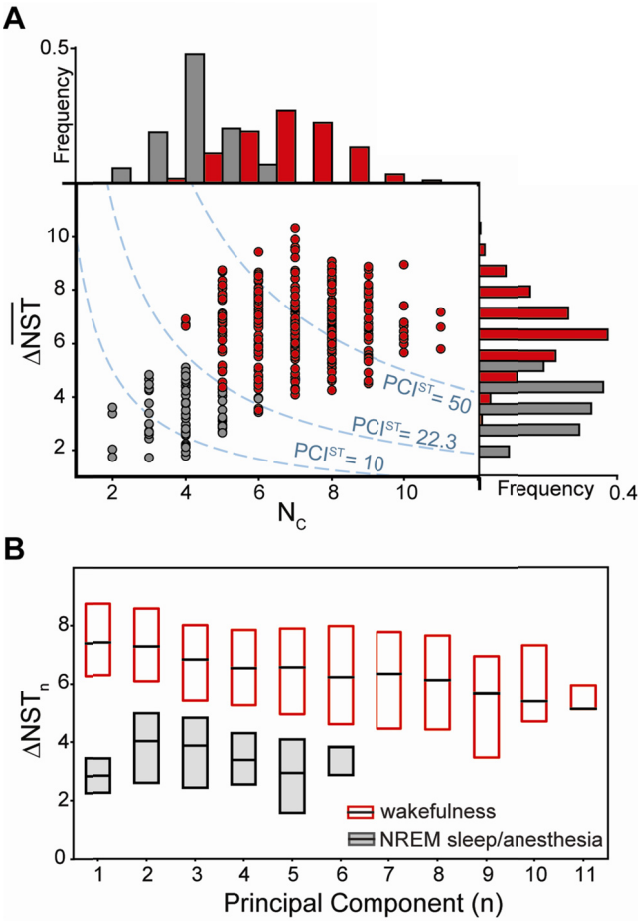

Fig 4. Spatiotemporal complexity is captured by PCIST through the number of selected components and the amount of state transitions for each component. (A) In the center, the relationship between the number of selected principal components (N_C) and the average number of state transitions across components ($\overline{\Delta NST}$) for all sessions in the benchmark recorded during consciousness (red) and unconsciousness (grey). The dotted blue lines correspond to the product of both quantities for different PCI_{ST} values ($PCI^{ST} = N_c \times \overline{\Delta NST}$). On the right and on the top are the histograms of the average NST and of number of selected principal components, respectively. (B) Relationship between selected principal component ordered by decreasing mean field power and the corresponding amount of state transitions for each component (ΔNST_n) (see Methods). Shown are the median and quartiles of ΔNST_n values for conscious (red) and unconscious (grey) conditions for the *n*th principal component, ranging from first to eleventh (as $N_C < 12$ for all sessions).

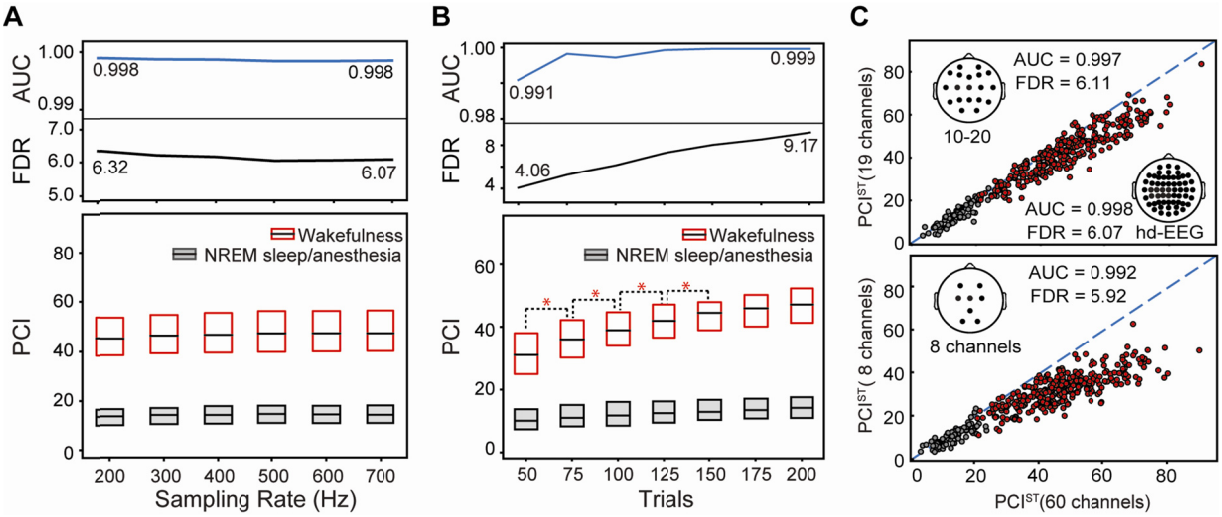

Fig 5. Dependence of PCIST on features of the TMS evoked potential. PCIST calculated on TMS evoked potentials recorded from conscious (wakefulness) and unconscious (NREM sleep/anesthesia) healthy individuals using different sampling frequencies, number of EEG channels and number of trials. (A) Influence of the signal's sampling frequency on PCIST obtained by downsampling the TEP signals. Shown are the boxplots with median and quartiles for conscious (red box) and unconscious (grey box) conditions, and corresponding classification power metrics (AUC and FDR) for sampling frequencies varying from 200Hz to 700Hz (top). (B) Dependence of PCIST on the number of trials (n_t) used to obtain the TMS evoked potential (TEP). For every session, surrogates TEP's were generated by randomly selecting n_t trials. The boxplots with median and quartiles (bottom) of the mean PCIST values across 25 surrogates for conscious (red box) and unconscious (grey box) conditions are displayed with corresponding FDR and AUC (top) for n_t ranging from 50 to 200 trials. Red asterisks indicate significant comparisons. (C) Pearson correlation between PCIST values for conscious (red) and unconscious (grey) conditions, with respective AUC and FDR values for the resulting distributions, calculated using the original hd-EEG system (horizontal axis) and two simpler EEG setups: a standard 10-20 EEG system (vertical axis, top panel) and a setup with 8 EEG channels (vertical axis, bottom panel).

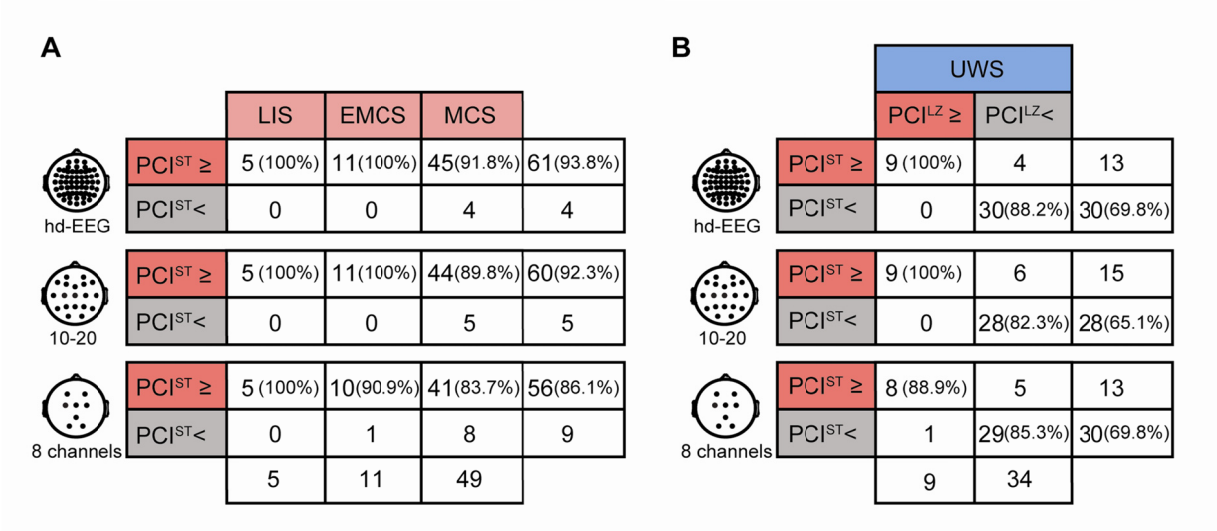

Fig 6. PCIST's ability to detect consciousness in brain-injured patients is preserved in simpler EEG setups. Number and percentages of patients classified as high (PCIST≥) and low (PCIST<) complexity with respect to the corresponding classification cutoffs obtained from the benchmark dataset are shown for EEG setups of 60 (top), 19 (middle) and 8 (bottom) channels. (A) PCIST's sensitivity in detecting signs of consciousness in conscious (LIS/EMCS) and minimally conscious (MCS) patients. (B) Contingency tables for the stratification of UWS patients in low complexity (PCI<) and high complexity (PCI≥) subgroups accordingly to PCI^{LZ} and PCIST.

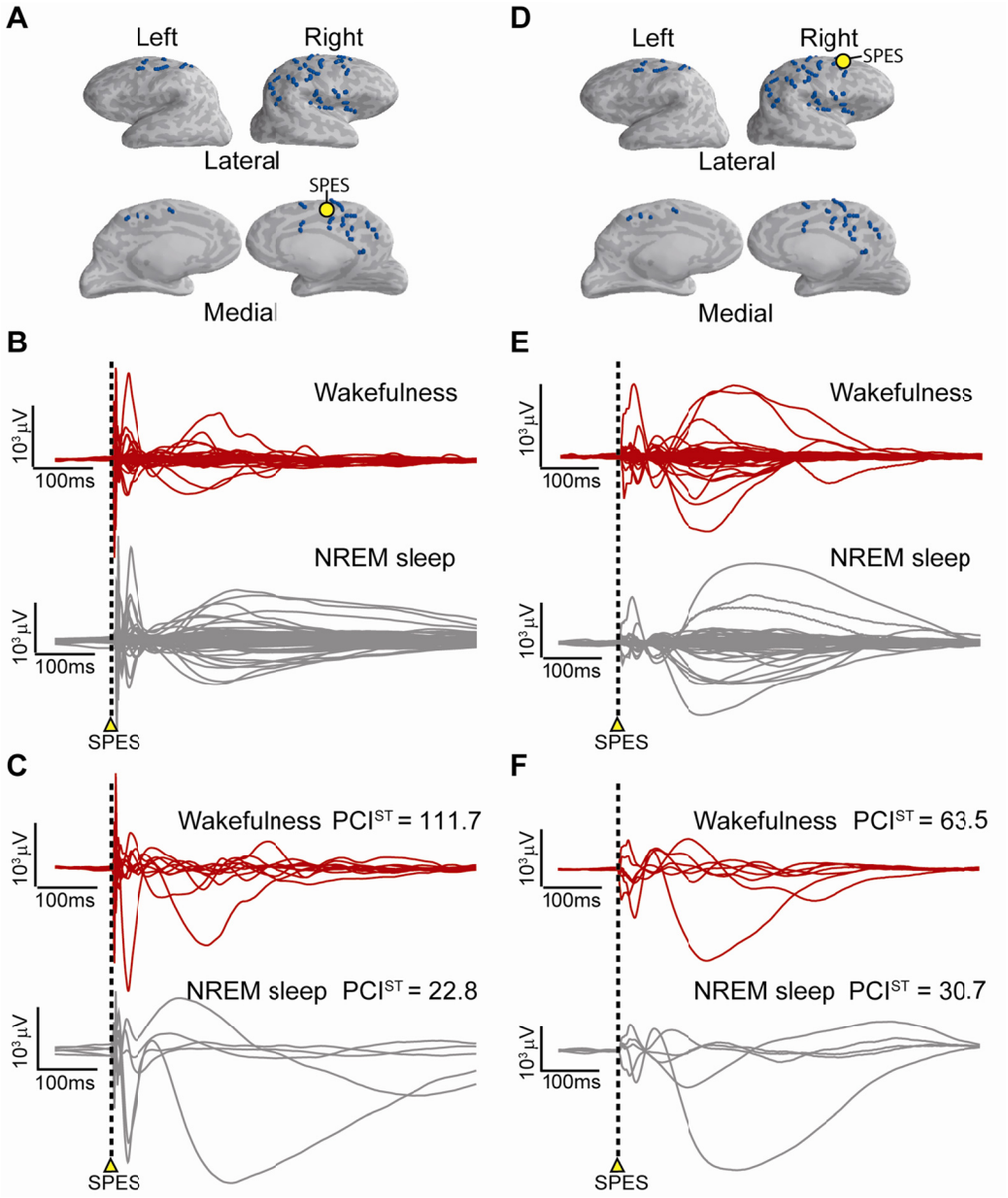

Fig 7. PCIST is able to quantify the spatiotemporal complexity of stereotactic EEG responses to SPES. SPES-evoked responses in the SEEG and principal component space are shown for a representative subject during stimulation delivered on the Superior Frontal Gyrus (panels A, B, C) and on the Superior Frontal Sulcus (panels D, E, F). Panels A and D depict the positions of the stimulating contact (yellow) and remaining SEEG contacts (blue) over a brain surface reconstructed from the individual's brain. The correspondent SPES/SEEG-evoked responses are shown in the respective middle

panels (B and E) as the superposition of the averaged SPES-evoked potentials recorded from all SEEG contacts during wakefulness (red traces) and NREM sleep (grey traces). Lower panels (C and F) depict the correspondent PCI^{ST} values and the SPES-evoked responses decomposed in principal components after dimensionality reduction.

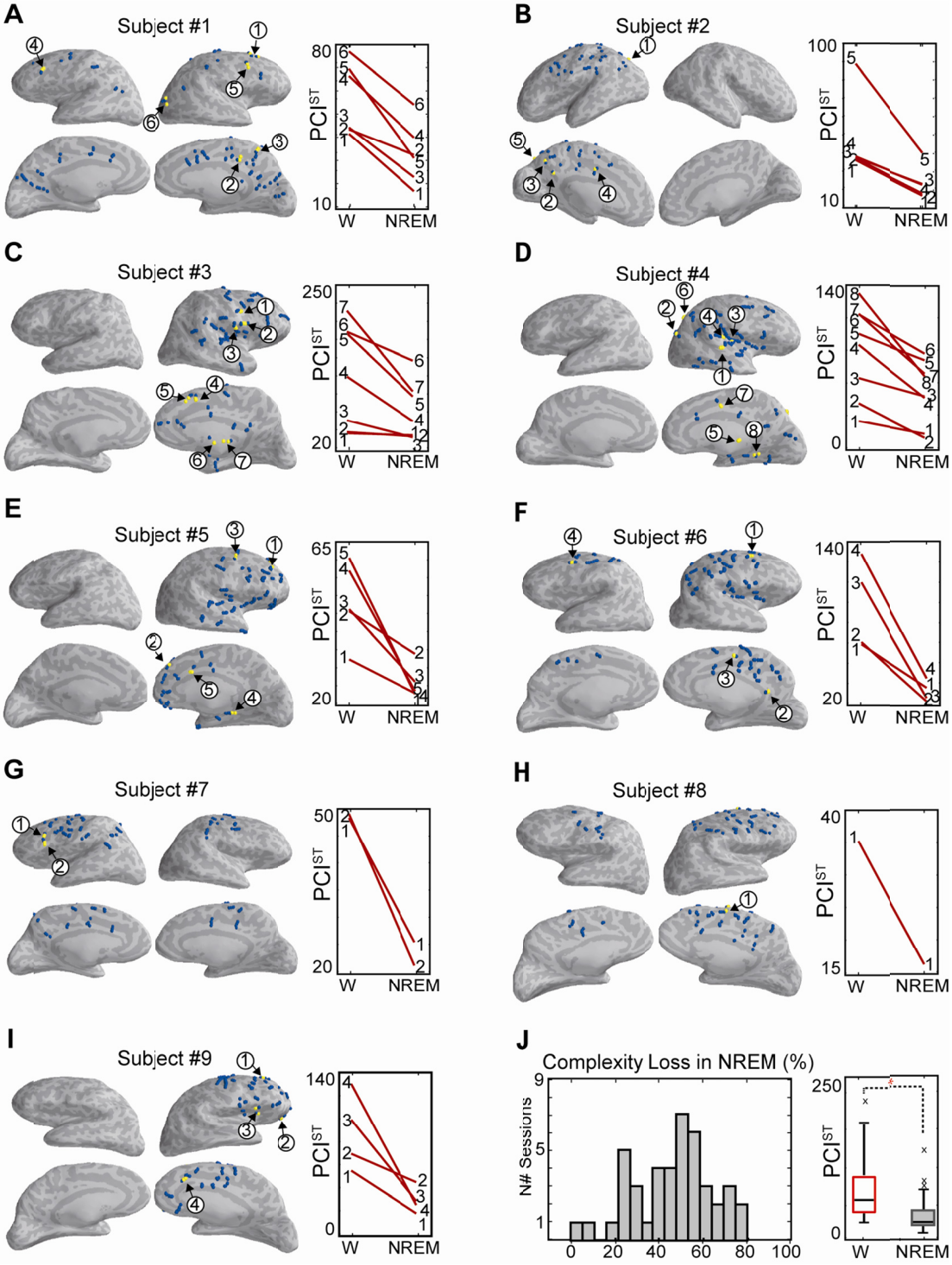

Fig 8. PCIST values in SPES-evoked potentials are invariably lower during NREM sleep as compared to wakefulness. Panels A – I: PCIST calculated in nine subjects during wakefulness (W) and NREM sleep are shown separately for each individual subject. SEEG (blue) and SPES contacts (yellow)

are depicted over brain surfaces reconstructed from the individual's brain (left). Numbers and arrows indicate the stimulation sites and the correspondent PCI^{ST} values (red traces, right). Panel J: shown are the percentage losses of complexity across all subjects and stimulation sites (left) and boxplots of PCI^{ST} values (right) at the group level for wakefulness (red box) and NREM sleep (grey box). Red asterisk indicate significant comparison ($p = 4.7 \times 10^{-7}$).